

## Article

# Response of Floods to the Underlying Surface Changes in the Taojiang River Basin Using the Hydrologic Engineering Center's Hydrologic Modeling System

Yong Xiao <sup>1,2</sup>, Tianfu Wen <sup>1,\*</sup>, Ping Gu <sup>2</sup>, Bin Xiong <sup>2</sup>, Fei Xu <sup>3</sup>, Junlin Chen <sup>1,4</sup> and Jiayu Zou <sup>1,2</sup>

<sup>1</sup> Key Laboratory of Poyang Lake Water Resources and Environment of Jiangxi Province, Jiangxi Academy of Water Science and Engineering, Nanchang 330029, China; 416000210041@email.ncu.edu.cn (Y.X.); 13155863167@163.com (J.C.); 416000210072@email.ncu.edu.cn (J.Z.)

<sup>2</sup> School of Infrastructure Engineering, Nanchang University, Nanchang 330031, China; guping@ncu.edu.cn (P.G.); xiongbin@ncu.edu.cn (B.X.)

<sup>3</sup> Guangzhou Institute of Geography, Guangdong Academy of Sciences, Guangzhou 510070, China; xufeigz@163.com

<sup>4</sup> College of Hydrology and Water Resources, Hohai University, Nanjing 210098, China

\* Correspondence: wen-tianfu@whu.edu.cn

**Abstract:** Due to underlying surface changes (USCs), the changes in the Taojiang River Basin's flood generation conditions could impact the flooding process in the basin. However, most studies have typically focused on either land-use changes (LUCs) or soil and water conservation measures (SWCMs) to assess the impact of the USCs on floods, which may not provide a more comprehensive understanding of the response of floods to the USCs. To investigate how the USCs have altered the floods in the Taojiang River Basin, located upstream of Poyang Lake, China, the HEC-HMS model, which incorporates the influence of the USCs into the parameter calibration, is established in this study to investigate the flood processes on an hourly scale. The flood peak and the maximum 72 h flood volume are selected as two indexes and are applied to analyze the changes in floods caused by the USCs. The 1981–2020 period is divided into three sub-periods (i.e., 1981–1992, 1993–2007, and 2008–2020) based on the conditions of the USCs. It is found that the two indexes have exhibited decreasing trends, mainly due to the USCs during 1981–2020. Benchmarked against the baseline period of 1981–1992, the two indexes decreased by 3.06% (the flood peak) and 4.00% (the maximum 72 h flood volume) during 1993–2007 and by 5.92% and 7.58% during 2008–2020. Moreover, the impacts of the LUCs and SWCMs are separated through parameter adjustments in the model, revealing that the SWCMs played a dominant role in the USCs in the Taojiang River Basin. The quantification and assessment of the impact of the USCs on floods of different magnitudes revealed that the influence decreases with increasing flood magnitude. The results of this study improve our understanding of how USCs affect the flooding process and therefore provide support for flood control management under changing environments.



**Citation:** Xiao, Y.; Wen, T.; Gu, P.; Xiong, B.; Xu, F.; Chen, J.; Zou, J. Response of Floods to the Underlying Surface Changes in the Taojiang River Basin Using the Hydrologic Engineering Center's Hydrologic Modeling System. *Water* **2024**, *16*, 1120. <https://doi.org/10.3390/w16081120>

Academic Editor: Enrico Creaco

Received: 2 March 2024

Revised: 1 April 2024

Accepted: 11 April 2024

Published: 15 April 2024



**Copyright:** © 2024 by the authors. Licensee MDPI, Basel, Switzerland. This article is an open access article distributed under the terms and conditions of the Creative Commons Attribution (CC BY) license (<https://creativecommons.org/licenses/by/4.0/>).

## 1. Introduction

Many environmental surface elements, such as the topography, land use, and soil type, influence the Taojiang River Basin's underlying surface conditions [1]. The hydrological properties of the basin's underlying surface have been impacted as a result of human activity, which has an impact on the condition of the flood generation in the basin [2]. The land-use changes (LUCs) are typically a direct manifestation of the underlying surface changes (USCs). The rapid growth of urbanization has increased the basin's impervious area, reducing rainfall infiltration and increasing the flood risk [3,4]. Zhao et al. [5] found

that urbanization would cause an increase in flood peak and flood volume, which has a significant amplification effect on designed flood. As urbanization levels rise, there is a more significant increase in the trend of flood peak and flood volume, which can result in a greater expansion of the flood risk areas [6]. Janizadeh et al. [7] predicted land-use scenarios for 2050 using the cellular automata (CA)–Markov model and used multiple machine-learning models and their integrated models to predict the future flood risk of the Kalvan Basin in Iran and found that urbanization would increase the proportion of the area at high risk by about 11% and the proportion of the area at very high risk by about 6%. The higher the level of urbanization, the greater the susceptibility to flooding. Contrary to the impact caused by urbanization, increased vegetation cover has a significant impact on reducing the runoff and flooding in small basins [8]. Vegetation intercepts rainwater and increases the surface roughness, resulting in less surface runoff [9]. Ghalehtemouri et al. [10] discovered that a large loss of forest trees in the city would lead to an increase in flooding in Kuala Lumpur. Gabriels et al. [11] estimated that an afforestation scheme of about  $1.88 \text{ km}^2$  in the Maarkebeek Basin could lower the flood risk by 57%. Therefore, increasing vegetation cover is crucial for flood control in the basin.

Similarly, soil and water conservation measures (SWCMs) have a significant impact on the USCs [12,13]. SWCMs can control soil erosion, improve the infiltration of rainfall, and increase the water storage capacity of the basin, so they play a significant role in reducing the extent of flooding during heavy rainfall events [14,15]. Zhao et al. [16] revealed that SWCMs can reduce the flood modulus by 57.2%, and they are the major driver of the flood changes in the Yellow River Basin under extreme rainfall conditions. Moreover, SWCMs such as terraces have been found to be more efficient in mitigating flooding compared to farmland and grassland [17]. In addition, the effectiveness of SWCMs in reducing runoff and flooding varies with the amount of rainfall. Zhu [18] demonstrated that in the Wangjiagou experimental basin, the effectiveness of SWCMs in reducing flood peaks ranged from 50.6% to 72.8% when the recurrence interval of the rainfall was 1–20 years, but it was significantly lower (only 15.8%) for rainfall with recurrence intervals of more than 20 years. While SWCMs are beneficial for flood control in the basin, their effectiveness is constrained by the treatment area.

The Taojiang River Basin, located in the upstream area of Poyang Lake, is one of the most serious areas of soil erosion in southern China [19]. Heavy rainfall is the primary cause of soil erosion in the Taojiang Basin, particularly during the high rainfall in the spring and summer months. The soil in the basin is mostly red soil with poor erosion resistance, which is prone to flash floods [20]. Since 1980, there has been significant urban expansion in the basin, which has resulted in an increase in soil erosion caused by urban construction. As a result, over the last four decades, a series of SWCMs have been implemented throughout the basin to control soil erosion [21]. In addition, urban development and SWCMs have contributed to the USCs in the basin and have affected the flooding process.

Hydrological models are an important tool for studying floods. The Hydrologic Engineering Center’s Hydrologic Modeling System (HEC-HMS) is a powerful and user-friendly semi-distributed hydrological model that has exceptional versatility in accommodating various basin sizes and time scales [22]. The practical applications of this model, such as runoff simulation [23,24], flood simulation [25,26], flash flood forecasting [27,28], and flood simulation in areas with little data [29,30], have been demonstrated to have remarkable efficacy. It can also be used to analyze the impact of USCs on floods [31,32]. Gao et al. [33] built the HEC-HMS model to simulate and predict the flooding process in the Qinhui River Basin in 2028 under different degrees of urbanization. Kabeja et al. [34] examined the changes in the flood peaks caused by afforestation in the Yanhe and Guangyuan river basins using the HEC-HMS model. Therefore, it is appropriate to use the HEC-HMS model to analyze the impact of USCs on flooding in the Taojiang River Basin.

Currently, numerous studies have investigated the impacts of USCs on floods and have primarily focused on either LUCs or SWCMs. However, this approach is not applicable in the Taojiang River Basin, in which the underlying surface changes are predominantly

influenced by a combination of both LUCs and SWCMs. By building the HEC-HMS model at an hourly scale, in this study, we quantified the response of floods to the USC<sub>s</sub> and separated the impacts of the LUCs and SWCMs through parameter adjustments. The results of this study improve our understanding of the impact of USC<sub>s</sub> on flooding and are of great significance for flood control in the Taojiang River Basin. In addition, limited research has been conducted on simulating the flooding process at an hourly scale in a large basin, and this study provides valuable support for its application in this area.

## 2. Study and Data

### 2.1. Study Area

The Taojiang River Basin, with a basin area of 7864 km<sup>2</sup>, is located in the southern region of Ganzhou City, Jiangxi Province, China, as the upstream area of the Poyang Lake Basin (Figure 1). The Taojiang River flows in a northerly direction from the basin. Julongtan Station is a hydrological station at the outlet of the basin, with a control area of 7715 km<sup>2</sup>, which is 98.6% of the total area of the basin. The basin contains a comprehensive river system, encompassing 10 first-class tributaries with catchment areas exceeding 200 km<sup>2</sup>, including the Taiping River, Wojiang River, Lianjiang River, and Huangtian River. It has a typical mid-subtropical humid monsoon climate characterized by prevailing winter and summer monsoon winds and notable temperature fluctuations. The basin's topography is dominated by mountains and hills, with significant terrain fluctuations. The predominant types of soil observed within the basin are red soil and brown-red soil. Regarding the land-use patterns, forest land such as horsetail pine forest, cedar forest, and moso bamboo pines dominates the landscape, followed by farmland. The average annual rainfall in the basin is 1595 mm, but due to the influence of the monsoon climate, there is an imbalanced spatial and temporal distribution of rainfall throughout the year. Heavy rainfall and floods are predominantly concentrated during April–June, and the storm centers are primarily distributed in the upper part of the basin [35].

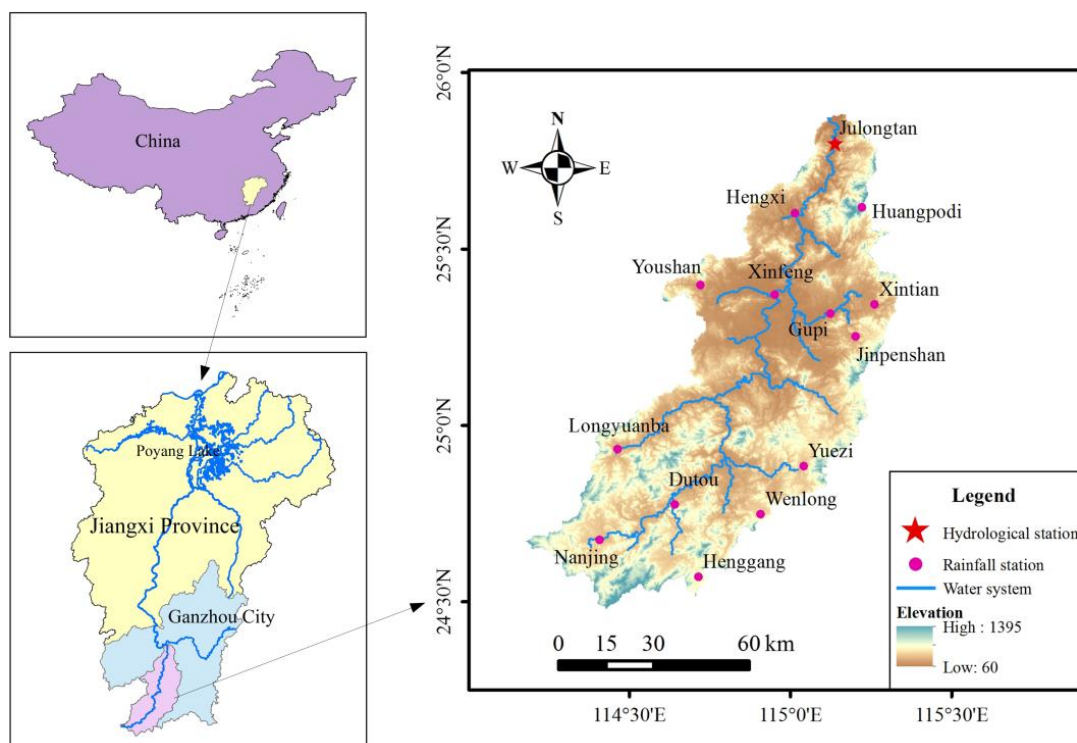


**Figure 1.** Location of the study area and distribution of hydrological stations and rainfall stations.

## 2.2. Data

The dataset utilized in this study includes a digital elevation model (DEM), land-use data, soil-type data, and rainfall and hydrological data. The DEM of the Taojiang River Basin was derived from the advanced spaceborne thermal emission and reflection radiometer (ASTER) global digital elevation model (GDEM) 30 m resolution digital elevation data from the Geospatial Data Cloud (<https://www.gscloud.cn/>). The land-use data were obtained from the PixelInformationExpert (PIE)-Engine remote sensing and geographic information cloud service platform (<https://engine.piesat.cn/>), and land-use data for 1985, 2000, and 2015 with a resolution of 30 m were selected. The soil-type data were derived from the Harmonized World Soil Database V1.2 (HWSD) created by the Food and Agriculture Organization of the United Nations (<https://www.fao.org/>), with a resolution of 1 km. The rainfall and hydrological data were obtained from the Hydrological Monitoring Centre of Jiangxi Province. The rainfall data included the extracts of the rainfall elements from 14 rainfall stations in the basin, including Julongtan, Xinfeng, and Dutou stations, spanning the period from 1981 to 2020. In addition, the hydrological data were extracts of the flood elements solely obtained from Julongtan Station during the same time period. (The extracts of the rainfall elements provide the observation records of each section of the major rainstorm events at the rain station, including the start and end time of each section and rainfall. The time interval of each segment is not fixed, but it is at the sub-day scale. It is the same for the extracts of the flood elements, which provide the major flood events observed by hydrological stations.) To achieve temporal alignment, the rainfall and flood data were uniformly discretized at an hourly time step.

## 3. Characteristic Analysis of the USCs

In the Taojiang River Basin, the USCs are mainly reflected in the SWCMs and LUCs under the influence of human activities. Due to the poor geological conditions in the basin and the frequent occurrence of heavy rainfall during the flood season, soil erosion in the basin has become very severe. To control soil erosion, a series of SWCMs have been carried out in the basin since the early 1980s, such as the treatment of collapsed hillocks, the transformation of terraces, and the sealing of forested areas in the mountains. Under the *High Quality Development Plan for Soil and Water Conservation in Ganzhou City (2021–2030)* issued by the Ganzhou Municipal Government, the area of soil and water erosion in Ganzhou City was reduced from 11,187 km<sup>2</sup> in 1980 to 6949 km<sup>2</sup> in 2020. The erosion area in the Taojiang River Basin decreased by about 547 km<sup>2</sup> from 1985 to 2000, accounting for 6.96% of the total area of the basin, and the erosion area decreased by about 750 km<sup>2</sup> from 1985 to 2015, accounting for 9.54% of the total area of the basin.

However, the overall LUCs in the Taojiang Basin were minor from 1985 to 2015 (Figure 2). As shown in Table 1, the main type of land use in the Taojiang River Basin was forest land, accounting for about 81% of the basin, followed by farmland, accounting for about 15%. In 2000, compared with 1985, the area of forest land increased by 2.50%, with an increase in the area of 157.68 km<sup>2</sup>; the area of farmland decreased by 11.07%, with a decrease in the area of 151.48 km<sup>2</sup>; the area of grassland decreased by 28.45 km<sup>2</sup>, and the areas of the built-up land and water increased by 19.82 and 2.88 km<sup>2</sup>, respectively. This indicates that during 1985–2000, the LUCs were primarily reflected by the conversion of farmland into forest land. In 2015, the forest land area decreased by 23.15 km<sup>2</sup> compared with 2000, while the farmland and grassland areas decreased by 8.23 and 11.99 km<sup>2</sup>, respectively. Conversely, the built-up land and water area increased by 40.10 and 3.30 km<sup>2</sup>, respectively. This indicates that during 2000–2015, the LUCs were primarily reflected in the increase in the area of built-up land due to urbanization. According to the aforementioned data, the areas of the forest land and farmland in the Taojiang River Basin changed considerably between 1985 and 2000, and then they became relatively stable, whereas the area of the built-up land, influenced by urbanization, exhibited an increasing trend, especially after 2000. The proportion of grassland and water areas in the basin was minor, and thus they made a relatively limited contribution to the LUCs within the basin.

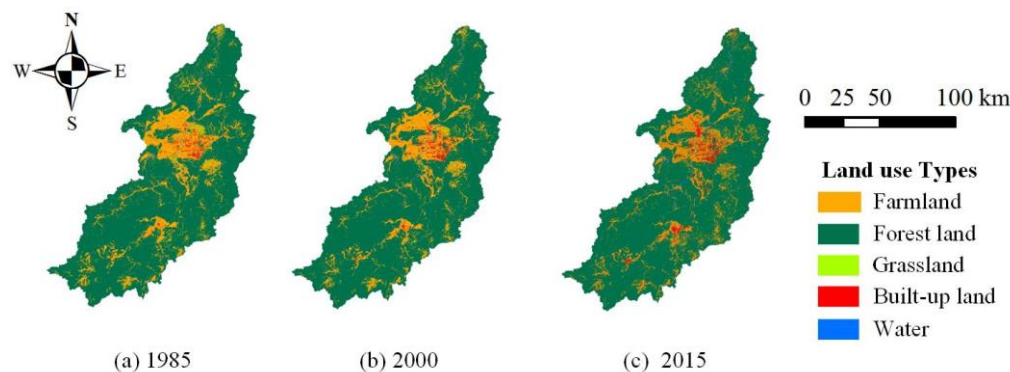


**Figure 2.** Land-use maps of the Taojiang River Basin in 1985, 2000, and 2015.

**Table 1.** Areas of land-use types in the Taojiang River Basin in 1985, 2000, and 2015.

Land-Use Types	1985		2000		2015	
	Area (km <sup>2</sup> )	Proportion (%)	Area (km <sup>2</sup> )	Proportion (%)	Area (km <sup>2</sup> )	Proportion (%)
Farmland	1367.87	17.39	1216.39	15.47	1208.16	15.36
Forest land	6312.65	80.27	6470.33	82.28	6447.18	81.98
Grassland	45.95	0.58	17.42	0.22	5.39	0.07
Built-up land	101.54	1.29	121.09	1.54	161.19	2.05
Water	36.00	0.46	38.78	0.49	42.08	0.54
Total	7864.00	100	7864.00	100	7864.00	100

#### 4. Methods

#### 4.1. HEC-HMS Model

According to the analysis of the USC presented in Section 3, forest land is the predominant land-use type in the Taojiang River Basin, which exceeds 80% of the total area. In fact, in the mid-1980s, extensive deforestation occurred in the Taojiang Basin. Subsequently, afforestation projects were implemented from 1993 to 2007 to restore forest cover, followed by a phase of forest regeneration. Therefore, we divided the period from 1981 to 2020 into three distinct sub-periods: the baseline period (1981–1992), the transition period (1993–2007), and the change period (2008–2020). The underlying surface conditions in 1985 were incorporated to simulate the floods during the baseline period, while those in 2000 and 2015 were used to represent the transition period and the change period, respectively. HEC-HMS models were constructed for the different periods, including ten typical floods and their corresponding rainfall events in each period.

The HEC-HMS model consists of a basin module, a meteorological module, a control module, and a time series module [36]. The main function of the basin module is to generalize the process of rainfall-induced runoff using the HEC-GeoHMS model in ArcGIS 10.2, which involves extracting the scope of the basin and the river network through DEM analysis, dividing the sub-basins, and calculating the characteristic parameters for both the sub-basins and river channels. In this study, the Taojiang River Basin was divided into 16 sub-basins, and 12 river channels were subsequently generated (Figure 3). The main function of the meteorological module is to determine the meteorological boundary conditions of the basin. The rainfall process in each sub-basin was computed using gage weights and Thiessen polygons based on the locations of the rainfall stations. The control module mainly determines the starting and stopping times of the model run and the time step, which was set to 1 h in this study. The time series module is primarily responsible for storing the input observation data for the rainfall and discharge, providing the basic data for the operation of the model.

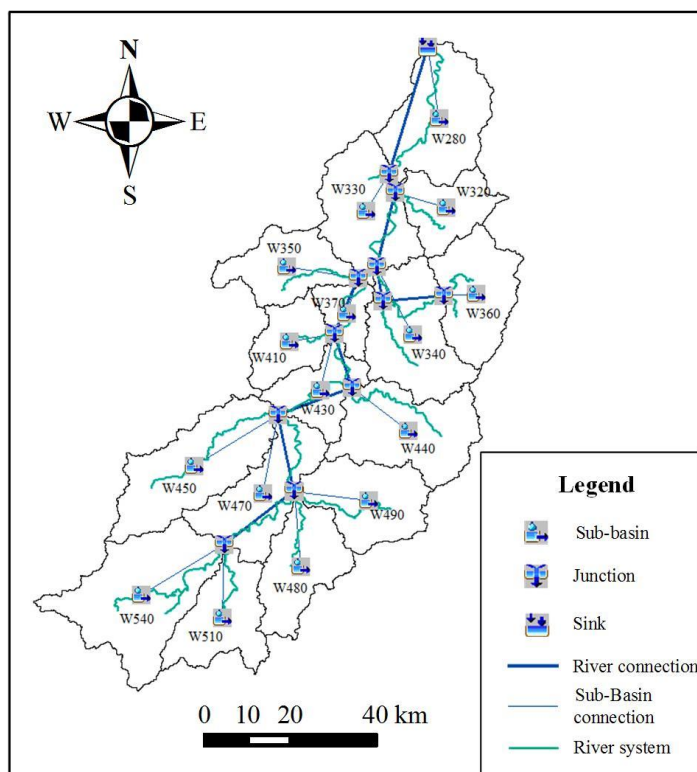


**Figure 3.** Diagram of the structure of the HEC-HMS model for the Taojiang River Basin.

In the basin module, the model divides the process of rainfall-induced runoff into four parts, namely, a loss model, transform model, base flow model, and routing model, providing a variety of calculation methods. A detailed description of each model is presented below.

#### 4.1.1. Loss Model

The loss model is mainly used to calculate the excess rainfall that forms runoff after the rainfall experiences natural processes such as plant interception, infiltration, and evaporation [37]. In this study, the Soil Conservation Service curve number (SCS-CN) method was chosen as the method for the loss model. This method has been widely used and is characterized by fewer parameters, consistent and reliable results, and strong physical significance. The calculation formula of this method is as follows:

$$P_e = \frac{(P - I_a)^2}{P - I_a + S} \quad (1)$$

where  $P_e$  is the excess rainfall (mm),  $P$  is the rainfall (mm),  $I_a$  is the initial rainfall loss (mm), and  $S$  is the potential maximum retention (mm). The following relationship exists between the initial rainfall loss ( $I_a$ ) and the potential maximum retention ( $S$ ):

$$I_a = \lambda S \quad (2)$$

where  $\lambda$  is the initial loss coefficient, which has an initial value of 0.05. The  $S$  can be expressed in terms of the curve number (CN):

$$S = \frac{25400 - 254CN}{CN} \quad (3)$$

where CN is a dimensionless parameter, and it is closely related to the basin soil type and land use. The soils were divided into four hydrological soil groups according to the

minimum infiltration rate: Group A (high infiltration rate), Group B (moderate infiltration rate), Group C (low infiltration rate), and Group D (lowest infiltration rate) [33]. Therefore, for the different soil types and land-use types in the basin, the table of CN values (Table 2) can be queried according to the land-use types and soil hydrological groups. Subsequently, the composite CN of each sub-basin can be calculated using the area weighting method and the following formula:

$$CN_{com} = \frac{\sum_{i=1}^n A_i CN_i}{\sum_{i=1}^n A_i} \quad (4)$$

where  $CN_{com}$  is the composite CN of the sub-basin,  $CN_i$  is the  $i$ th CN of the sub-basin, and  $A_i$  is the area of the  $i$ th CN in the sub-basin.

**Table 2.** The CNs of the different land-use types and soil hydrological groups.

Land-Use Types	Soil Hydrological Groups			
	A	B	C	D
Farmland	65	75	82	86
Forest land	25	55	70	77
Grassland	30	58	71	78
Built-up land	69	80	86	90
Water	92	92	92	92

In addition, *imperviousness* is an important parameter in the SCS-CN method, which is usually determined by the area weight of the built-up land in the basin [38]. The CN and *imperviousness* of each sub-basin in the Taojiang River Basin during the different periods are listed in Table 3.

**Table 3.** CN and *imperviousness* values for the sub-basins in 1985, 2000, and 2015.

Sub-Basin Number	CN of Sub-Basin			Imperviousness of Sub-Basin (%)		
	1985	2000	2015	1985	2000	2015
W490	57.66	57.74	58.71	0.29	0.57	1.49
W480	59.20	58.48	59.85	0.63	1.04	2.69
W470	57.74	57.47	57.64	0.71	0.82	0.93
W450	56.45	56.14	56.41	0.10	0.13	0.19
W440	57.29	57.25	57.71	0.27	0.39	0.96
W430	60.62	59.77	59.57	0.76	0.99	1.32
W410	66.41	65.01	64.31	2.48	2.87	3.26
W370	73.00	71.39	70.57	11.40	13.13	14.84
W360	56.78	56.72	57.01	0.28	0.32	0.49
W350	66.50	65.4	64.79	2.04	2.75	3.75
W340	64.31	63.72	62.92	6.62	7.31	7.64
W330	61.37	60.98	60.86	1.02	1.23	2.22
W320	57.71	58.06	58.08	0.29	0.41	0.60
W540	57.87	57.38	57.64	0.40	0.50	0.98
W510	57.07	56.94	56.97	0.19	0.27	0.41
W280	57.48	57.25	57.3	0.32	0.34	0.48

#### 4.1.2. Transform Model

The transform model was used to calculate the direct runoff formed at the outlet of the basin by the excess rainfall [39]. The Snyder unit line method was chosen as the transform model in this study, which has fewer parameters and easy calculations. The Snyder unit line method has defined standard unit lines, and the flood peak, lag time, and rainfall durations are used as the characteristic values of the watershed. The main parameters of the Snyder unit line method are the lag time ( $t_p$ ) and the peaking coefficient ( $C_p$ ). In

practical applications, the  $t_p$  can usually be calculated according to the formula derived from the relationship between the watershed parameters such as the longest catchment path, basin slope, and hydrological characteristics of the basin:

$$t_p = CC_t(LL_c)^{0.3} \quad (5)$$

where C is the conversion coefficient (set as 2 in this study);  $C_t$  is the basin coefficient, ranging from 1.8 to 2.2, with an initial value of 2; L is the length of the main river (km); and  $L_c$  is the length from the center of mass of the basin to the outlet of the basin (km). Due to the fact that  $C_t$  and  $C_p$  are not physically based parameters,  $t_p$  and  $C_p$  need to be determined by parameter optimization.

#### 4.1.3. Base Flow Model

The recession model was selected as the base flow model. It is an exponential decay model based on the existence of a certain relationship between the base flow at any time and the base flow at the initial time:

$$Q_t = Q_0 k^t \quad (6)$$

where  $Q_t$  is the base flow at time  $t$  ( $\text{m}^3/\text{s}$ ),  $Q_0$  is the base flow at the initial time ( $\text{m}^3/\text{s}$ ), and  $k$  is the recession constant.

#### 4.1.4. Routing Model

The Muskingum method was chosen for the routing model. It is a river routing calculation method based on the water balance equation and the tank storage equation, with few parameters and high accuracy [40]. The formulas are as follows:

$$Q_t = C_1 I_t + C_2 I_{t-1} + C_3 Q_{t-1} \quad (7)$$

$$\begin{cases} C_1 = \frac{\Delta t - 2KX}{2K(1-X) + \Delta t} \\ C_2 = \frac{\Delta t + 2KX}{2K(1-X) + \Delta t} \\ C_3 = \frac{2K(1-X) - \Delta t}{2K(1-X) + \Delta t} \end{cases} \quad (8)$$

where  $Q_t$  and  $Q_{t-1}$  are the outflow from the river cross-section at time  $t$  and time  $t - 1$ , respectively;  $I_t$  and  $I_{t-1}$  are the inflow from the river cross-section at time  $t$  and time  $t - 1$ , respectively;  $K$  is the movement time of the flood in the river channel;  $X$  is the flow specificity factor, which is generally within the range of 0–0.5; and  $\Delta t$  is the time step of the calculation.

#### 4.2. Model Evaluation

To improve the simulation results, the model parameters were optimized using the built-in univariate gradient of the model as an optimization method and the peak-weighted root mean square error as the objective function. This approach was complemented by a manual trial-and-error method. When assessing the model effect, according to the *Standard for hydrological information and hydrological forecasting* (GB/T22482-2008) [41], four evaluation indexes, namely the flood peak relative error (REP), flood volume relative error (REV), peak present time error ( $\Delta t$ ), and deterministic coefficient (DC), were used to evaluate the single-field flood. The formulas for each of the evaluation indexes are as follows:

$$REP = \frac{(P_c - P_o)}{P_o} \times 100\% \quad (9)$$

$$REV = \frac{(V_c - V_o)}{V_o} \times 100\% \quad (10)$$

$$\Delta t = T_c - T_o \quad (11)$$

$$DC = 1 - \frac{\sum_{i=1}^n [y_c(i) - y_o(i)]^2}{\sum_{i=1}^n [y_o(i) - \bar{y}_o]^2} \quad (12)$$

where  $P_c$  and  $P_o$  are the simulated and observed flood peaks ( $\text{m}^3/\text{s}$ ), respectively;  $V_c$  and  $V_o$  are the simulated and observed flood volumes (mm), respectively;  $T_c$  and  $T_o$  are the peak occurrence times of the simulated and observed flood processes, respectively;  $y_c(i)$  and  $y_o(i)$  are the simulated and observed discharges at moment  $i$  ( $\text{m}^3/\text{s}$ ), respectively; and  $\bar{y}_o$  is the average observed discharge ( $\text{m}^3/\text{s}$ ). For a single flood event, according to the specification, the forecast error is considered acceptable if it falls within the permissible range. Specifically, both  $REP$  and  $REV$  should be within 20%, and  $\Delta t$  must not exceed three hours. The multiple forecasts were evaluated using the qualification rate ( $QR$ ), which is the ratio of the number of qualified forecasts to the total number of forecasts. The flood forecasting accuracy of the model can be determined according to the  $QR$  or the  $DC$  (Table 4).

**Table 4.** Flood forecasting accuracy level.

Accuracy Level	A	B	C
$QR$ (%)	$QR \geq 85$	$85 > QR \geq 70$	$70 > QR \geq 60$
$DC$	$DC > 0.9$	$0.9 \geq DC \geq 0.7$	$0.7 > DC \geq 0.5$

#### 4.3. Flood Simulation Methods for Various Underlying Surface Scenarios

To mitigate the influences of the spatiotemporal distribution and magnitude of the rainfall on the results, a total of 30 rainfall events were chosen for flood simulation in this study, including various underlying surface conditions. The differences observed in the flood simulation results across the various scenarios can be attributed to the impacts of the USC, with the flood peak and the maximum 72 h flood volume as two indexes for quantifying the impacts. It should be noted that the objective of this study was to analyze the impacts of the USC, and the input historical rainfall events were kept constant across the various USC scenarios.

In this study, the USC were considered the results of the combined effects of the LUCs and SWCMs. The three sets of parameter scenarios obtained using the HEC-HMS model to simulate the floods during the three periods, namely, the baseline, transition, and change periods, reflect the underlying surface conditions during the three periods. The model parameters  $CN$  and *imperviousness* can effectively capture the land-use conditions, and both can be directly determined, enabling separation of the impacts of the LUCs and SWCMs on the floods. Therefore, the parameters can be adjusted to establish various underlying surface scenarios. According to the land use and soil erosion conditions during the different periods, nine distinct scenarios representing the underlying surface variations were established (Table 5). Among them, the impact of the USC on the floods can be expressed as follows:

$$I_{2000USCs} = S_5 - S_1 \quad (13)$$

$$I_{2015USCs} = S_9 - S_1 \quad (14)$$

where  $I_{2000USCs}$  and  $I_{2015USCs}$  indicate the impacts of the USC on the floods during the transition and change periods compared with the baseline period, respectively. The impact of the LUC on the floods can be expressed as follows:

$$I_{2000LUCs} = (S_2 - S_1) + (S_5 - S_4) + (S_8 - S_7) \quad (15)$$

$$I_{2015LUCs} = (S_3 - S_1) + (S_6 - S_4) + (S_9 - S_7) \quad (16)$$

where  $I_{2000LUCs}$  and  $I_{2015LUCs}$  are the impacts of the LUC on the floods during the transition and the change periods compared with the baseline period, respectively. Notably, LUCs

simulation scenarios S1, S5, and S9 only included ten flood events during the corresponding period. However, the model parameters could not directly reflect the changes during the periods before and after the SWCMs were implemented due to the various effects of the different SWCMs. Therefore, in this study, the difference between the impacts of the USCs and LUCs on the floods was calculated and used to determine the impact of the SWCMs on the floods:

$$I_{2000SWCMs} = I_{2000USCs} - I_{2000LUCs} \quad (17)$$

$$I_{2015SWCMs} = I_{2015USCs} - I_{2015LUCs} \quad (18)$$

where  $I_{2000SWCMs}$  is the impact of the SWCMs on the floods between the transition period and the baseline period, and  $I_{2015SWCMs}$  is the impact of the SWCMs on the floods between the change period and the baseline period.

**Table 5.** The different settings of the underlying surface scenarios.

Scenario Name	Scenario Settings	Participation during Simulated Flood Events
S1	Soil erosion conditions in 1985 + land-use conditions in 1985	All thirty events
S2	Soil erosion conditions in 1985 + land-use conditions in 2000	Ten events during the baseline period
S3	Soil erosion conditions in 1985 + land-use conditions in 2015	Ten events during the baseline period
S4	Soil erosion conditions in 2000 + land-use conditions in 1985	Ten events during the transition period
S5	Soil erosion conditions in 2000 + land-use conditions in 2000	All thirty events
S6	Soil erosion conditions in 2000 + land-use conditions in 2015	Ten events during the transition period
S7	Soil erosion conditions in 2015 + land-use conditions in 1985	Ten events during the change period
S8	Soil erosion conditions in 2015 + land-use conditions in 2000	Ten events during the change period
S9	Soil erosion conditions in 2015 + land-use conditions in 2015	All thirty events

## 5. Results and Analysis

### 5.1. Evaluation and Analysis of Flood Simulation

In this study, the calibration process involved six floods selected from each period, while the remaining four floods were used for the verification. According to the simulation results (Table 6), the overall simulation results for all three periods are relatively satisfactory. Among the 30 simulated floods, only two floods had  $REP$  values of  $>20\%$ , while seven floods had  $\Delta t$  values of greater than three hours. Conversely, the  $REV$  values of all of the floods remained within 20%. Notably, the simulated peak of flood No. 19870517 (the flood events are named based on their occurrence date of the flood peak, including the day, month, and year) was smaller due to a preceding rainfall event, which resulted in an increased initial soil moisture content and subsequently reduced the amount of rainfall loss, leading to a lower simulated value. The simulated  $\Delta t$  value of flood No. 19920328 was excessively large due to its nature as a double-peak flood, with the first peak being slightly larger than the second peak. However, it should be noted that the simulated flood peak aligned more closely with the observed second peak. In addition, the HEC-HMS model had limited efficacy in simulating multi-peak floods (Figures 4 and 5). This is attributed to the utilization of the Snyder unit line method in the transform model, which is primarily designed for standard single-peak flood scenarios and thus is inadequate for accurately representing multi-peak floods [42]. The  $QR$  values of the flood simulations during these three periods were 80%, 70%, and 70%, and the average  $DC$  value was greater than 0.7, resulting in a Grade B forecasting accuracy. This suggests that the HEC-HMS model is well suited for application in the Taojiang River Basin.

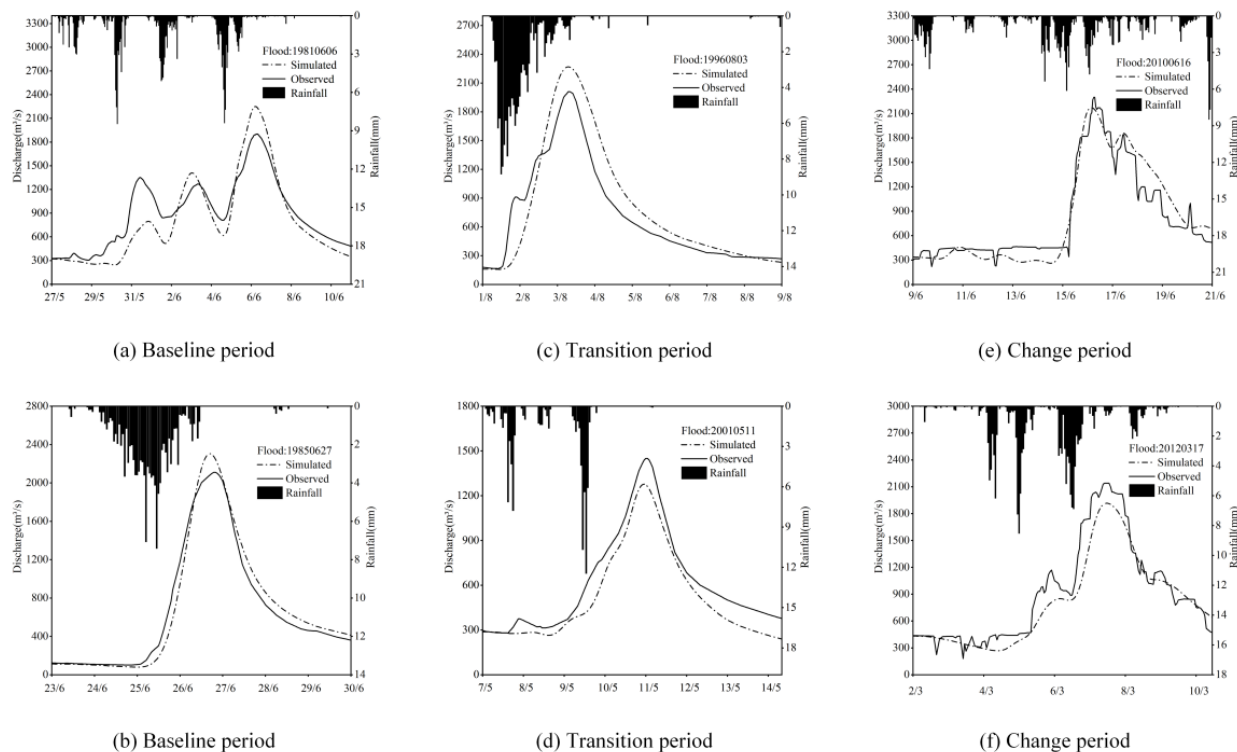


**Figure 4.** Observed and simulated flooding processes for calibration during the (a,b) baseline, (c,d) transition, and (e,f) change periods.

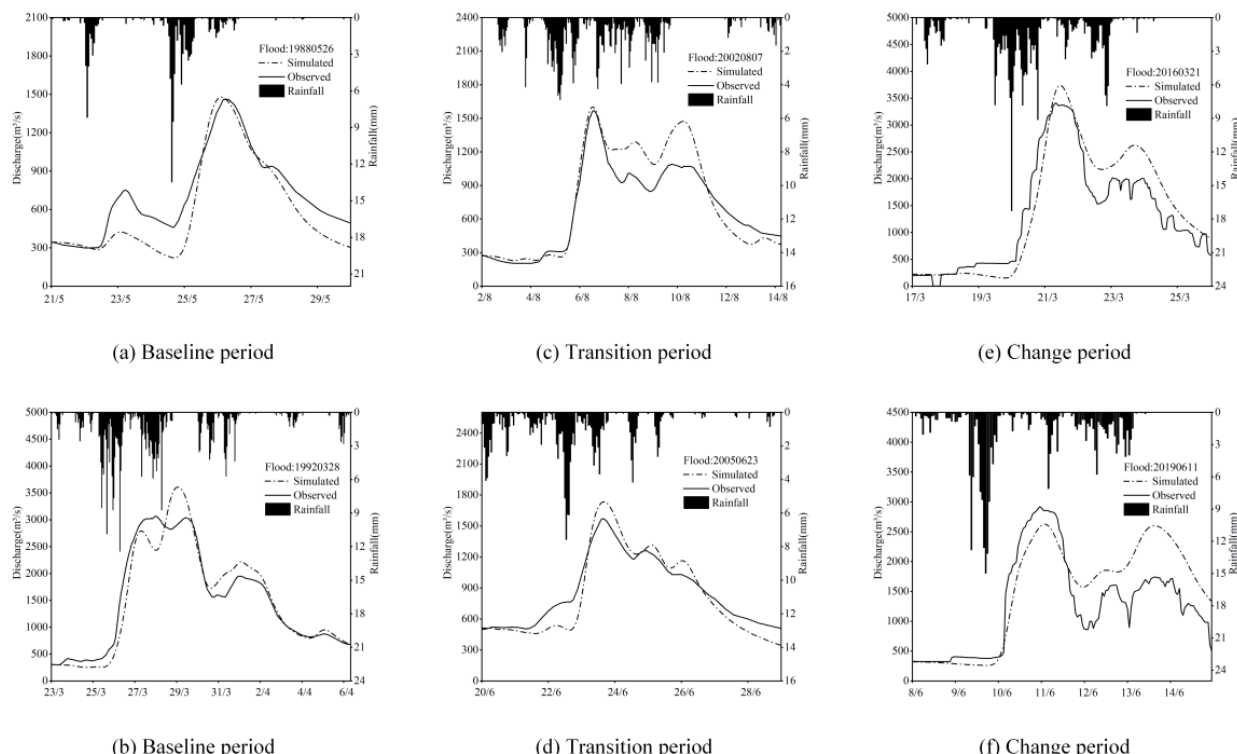


**Figure 5.** Observed and simulated flooding processes for verification during the (a,b) baseline, (c,d) transition, and (e,f) change periods.

**Table 6.** Flood simulation results in the baseline, transition, and change periods.

Simulation Periods	Flood Number	REP (%)	REV (%)	$\Delta t$ (h)	DC	Qualified (Q)/ Failed (F)
Baseline period	19810606	18.44	-9.89	-1	0.71	Q
	19840428	-12.60	-15.05	1	0.91	Q
	19850627	9.24	2.98	-2	0.97	Q
	19850925	3.14	13.06	-1	0.94	Q
	19860606	8.95	8.87	-2	0.79	Q
	19870517	-26.68	-19.18	1	0.84	F
	19880526	1.27	-16.19	-1	0.84	Q
	19890523	-16.38	-13.36	-2	0.93	Q
	19900412	-15.45	-13.97	-1	0.89	Q
	19920328	17.53	0.02	26	0.92	F
	19940621	28.06	8.81	-8	0.90	F
	19950618	-0.96	6.81	-8	0.93	F
Transition period	19960803	12.89	12.42	0	0.79	Q
	19980310	4.56	-5.32	-2	0.82	Q
	20010511	-11.89	-15.68	-1	0.88	Q
	20020807	2.04	9.87	-1	0.80	Q
	20030519	-5.95	-10.27	-5	0.90	F
	20040408	8.18	14.71	-1	0.85	Q
	20050623	10.42	-3.73	1	0.85	Q
	20060523	-12.56	-15.09	0	0.85	Q
Change period	20080614	-5.84	6.50	1	0.90	Q
	20090704	13.65	12.69	5	0.92	F
	20100616	-5.55	2.44	-2	0.90	Q
	20110517	14.70	9.56	3	0.92	Q
	20120317	-10.49	-10.20	1	0.90	Q
	20150521	-1.37	5.12	5	0.82	F
	20160321	9.67	9.18	3	0.84	Q
	20190310	8.04	2.12	2	0.61	Q
	20190611	-9.96	16.29	3	0.60	Q
	20200404	6.52	15.83	6	0.78	F

Note: Positive values of the peak present time error indicate that the simulated flood peak was later than the observed flood time, while negative values indicate that the simulated flood peak was earlier than the observed flood time.

### 5.2. Response of Floods to USCs

The sensitivities to the parameters of the model vary among different floods [40,43]. Using a small sample size of flood events to investigate the impact of USCs on floods may potentially introduce bias and distort the research results. The method described above was employed to utilize the different model parameters to represent the different underlying surface conditions. All 30 flood events were incorporated into the various scenario simulations, and the resulting simulations were averaged to obtain final results that more realistically reflected the impact of the USCs on the floods. The two indexes, i.e., the flood peak and the maximum 72 h flood volume, were used to illustrate the difference between the various scenarios. Table 7 displays the average values of the flood peak and maximum 72 h flood volume for the 30 simulated floods obtained under scenarios S1, S5, and S9 (some simulation results are shown in Table A1). From 1981 to 2020, the USCs resulted in decreasing trends for both the flood peak and the maximum 72 h flood volume in the Taojiang River Basin. Compared with the baseline period, the peak and maximum 72 h flood volume decreased by 3.06% and 4.00% in the transition period and by 5.92% and 7.58% in the change period, respectively.

**Table 7.** The impact of the USC<sub>s</sub> on floods.

Simulation Periods	Average Flood Peak (m <sup>3</sup> /s)	Average Maximum 72 h Flood Volume (mm)	Relative Change in Flood Peak (%)	Relative Change in Maximum 72 h Flood Volume (%)
Baseline period	2240	52.13	-	-
Transition period	2178	50.27	-3.06	-4.00
Change period	2122	48.72	-5.92	-7.58

Table 8 presents the impact of the LUC<sub>s</sub> on floods by simulating ten flood events during the corresponding periods under scenarios S1–S9 (some simulation results are shown in Table A2). The trends of the impacts of the LUC<sub>s</sub> on the flood peak and maximum 72 h flood volume initially decreased and then increased. The flood peak and maximum 72 h flood volume decreased by 0.66% and 0.59% during the transition period, respectively, and increased by 0.11% and 0.20% during the change period. A comparison was made between the land use in 1985 and 2000. The primary differences occurred in the large area of the returning farmland to forest project, and the forest land had a lower CN value compared with the farmland. Given the positive correlations between the CN and flood peak and flood volume, the transition period resulted in decreases in the flood peaks and maximum 72 h flood volume [44]. The LUC<sub>s</sub> observed between 2000 and 2015 primarily involved the conversion of farmland, forest land, and grassland into higher CN built-up land and water, with a significant increase in the area of built-up land. This process was accompanied by an increase in the *imperviousness* value of the basin, which was positively correlated with the flood peak and volume [45]. Therefore, there were increases in the flood peak and maximum 72 h flood volume during the change period compared with the transition period.

**Table 8.** The impacts of the LUC<sub>s</sub> and the SWCMs on floods.

Simulation Periods	LUC <sub>s</sub>				SWCMs		
	Average Flood Peak (m <sup>3</sup> /s)	Average Maximum 72 h Flood Volume (mm)	Relative Change in Flood Peak (%)	Relative Change in Maximum 72 h Flood Volume (%)	Relative Change in Flood Peak (%)	Relative Change in Maximum 72 h Flood Volume (%)	Relative Change in Maximum 72 h Flood Volume (%)
Baseline period	2186	50.48	-	-	-	-	-
Transition period	2172	50.18	-0.66	-0.59	-2.40	-3.41	-
Change period	2187	50.54	0.11	0.20	-6.03	-7.78	-

According to the method outlined in Section 4.3, we determined the impact of the SWCMs on the floods (Table 8). The flood peak and maximum 72 h flood volume consistently decreased due to the SWCMs. Compared with the baseline period, during the transition period, these two indexes decreased by 2.40% and 3.41%, respectively, and they decreased by 6.03% and 7.78% during the change period, respectively. Based on the impacts of the USC<sub>s</sub> and the LUC<sub>s</sub>, it was concluded that the SWCMs were the primary factors contributing to the reductions in the flood peak and volume in the basin, and they played a dominant role in the USC<sub>s</sub> in the basin. In addition, the SWCMs had a more significant impact on the flood volume than the flood peak. This is attributed to their ability to reduce the surface runoff and enhance the soil permeability within the treated areas, all of which had significant impacts on the flood volume.

### 5.3. Analysis of the Response of Floods of Different Magnitudes to USC

Scatter plots were generated and fitted based on the relationship between the relative changes in the flood peak and maximum 72 h flood volume and their own magnitudes (Figure 6). The impacts of the USC, the LUCs, and the SWCMs on the floods gradually decreased with increasing flood magnitude. Generally, the magnitude of the floods was closely correlated with the magnitude of the rainfall [46]. In the loss model,  $I_a$  of each rainfall event was kept constant under the same underlying surface conditions. The amount of rainfall loss is influenced by the USC. Consequently, the small rainfall events exhibited a higher proportion of rainfall loss compared with the large events, and thus the small events had a greater overall impact. The phenomenon was also reflected in the flood process, which was embodied in the relative change in flood peak and flood volume. However, the relationship between the impact of the LUCs on the floods and flood magnitude remained very small during the transition period, which could be attributed to the minor changes in the imperviousness values observed within the context of overall limited LUCs. Compared with 1985, the increase in the built-up land in 2000 was relatively small, resulting in a smaller *imperviousness* value and an insignificant relationship between the impact of the LUCs on the floods and the flood magnitude. By contrast, there was a significant increase in the built-up land in 2015, resulting in a corresponding increase in the *imperviousness* value. Consequently, the impact of the LUCs on the floods decreased with increasing flood magnitude. However, the limited extent of the LUCs and the instability of their impact on the floods contributed to this result.

To further quantify the impact of the USC on the floods of different magnitudes, based on their flood peak discharges, the 30 historical flood events used in this study were classified into three magnitude levels: eight large floods (peak discharges of  $>2700 \text{ m}^3/\text{s}$ ), ten medium floods (peak discharges of  $2000\text{--}2700 \text{ m}^3/\text{s}$ ), and twelve small floods (peak discharges of  $<2000 \text{ m}^3/\text{s}$ ). As can be seen from Figure 7 and Table A3, the USC resulted in flood peak decreases of 4.03%, 2.75%, and 2.00% for the small, medium, and large floods during the transition period compared with the baseline period, respectively, and decreases of 5.19%, 3.48%, and 2.87% in the maximum 72 h flood volume, respectively. Similarly, during the change period the flood peaks decreased by 8.15%, 5.06%, and 3.64%, and the maximum 72 h flood volume decreased by 10.47%, 6.27%, and 4.89%.

During the transition period, for the small, medium, and large floods, the LUCs resulted in decreases in the flood peaks of 0.67%, 0.68%, and 0.61%, respectively, and decreases in the maximum 72 h flood volume of 0.59%, 0.60%, and 0.59%, respectively. During the change period, the flood peaks of small floods increased by 0.40%, while the flood peaks of the medium and large floods slightly decreased by 0.13% and 0.03%, respectively. However, the maximum 72 h flood volume increased by 0.49% for the small floods, increased by only 0.03% for the medium floods, and slightly decreased by 0.02% for the large floods.

The implementation of SWCMs led to reductions of 3.36%, 2.07%, and 1.38% in the flood peaks of the small, medium, and large floods during the transition period, respectively, and decreases of 4.60%, 2.87%, and 2.29% in the maximum 72 h flood volume, respectively. During the change period, the flood peaks decreased by 8.55%, 4.93%, and 3.61%, and the maximum 72 h flood volume decreased by 10.96%, 6.29%, and 4.87%.

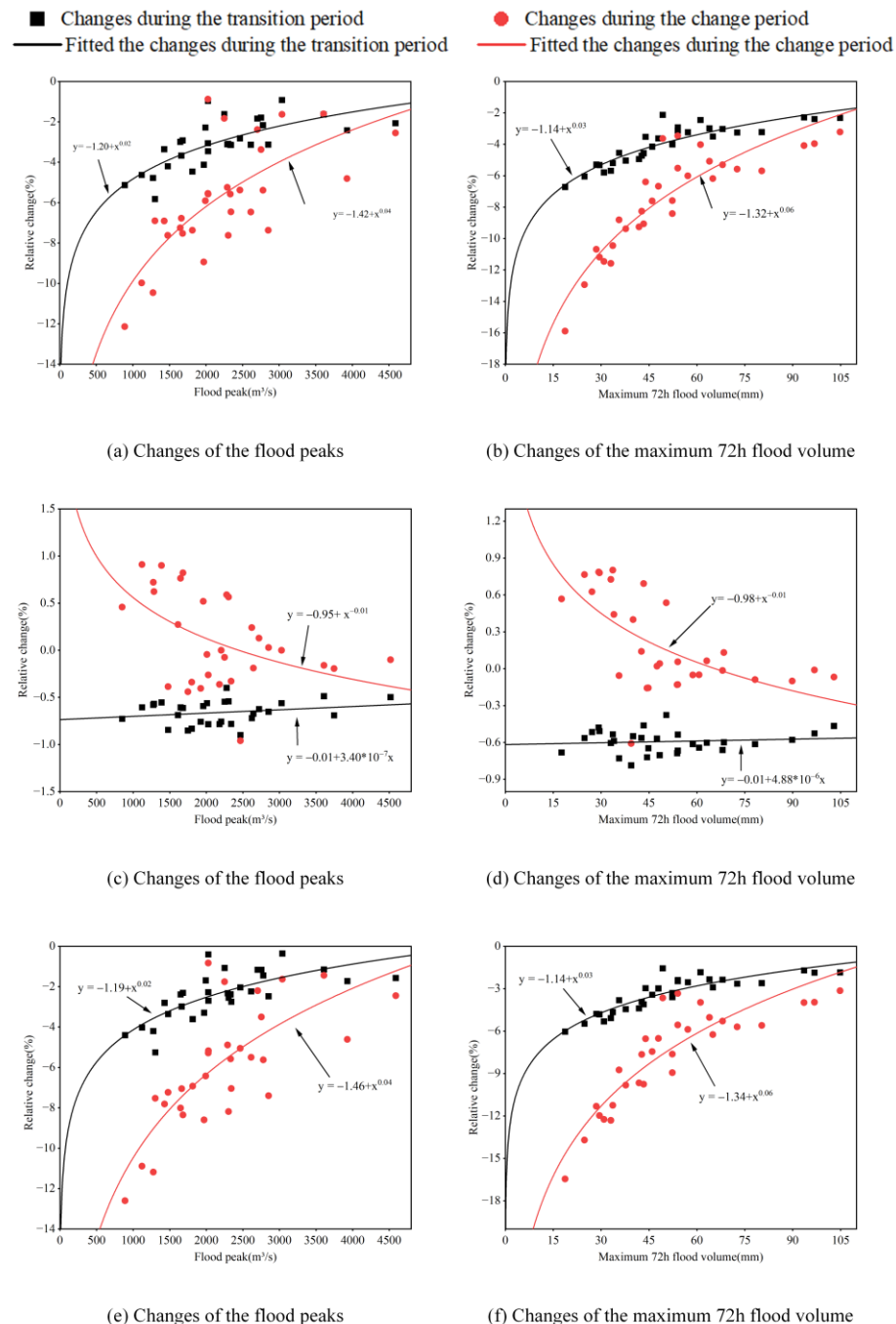


**Figure 6.** The relationship between the relative changes in the flood peak and maximum 72 h flood volume and their own magnitudes under different scenarios: **(a,b)** USC; **(c,d)** LUCs; **(e,f)** SWCMs.

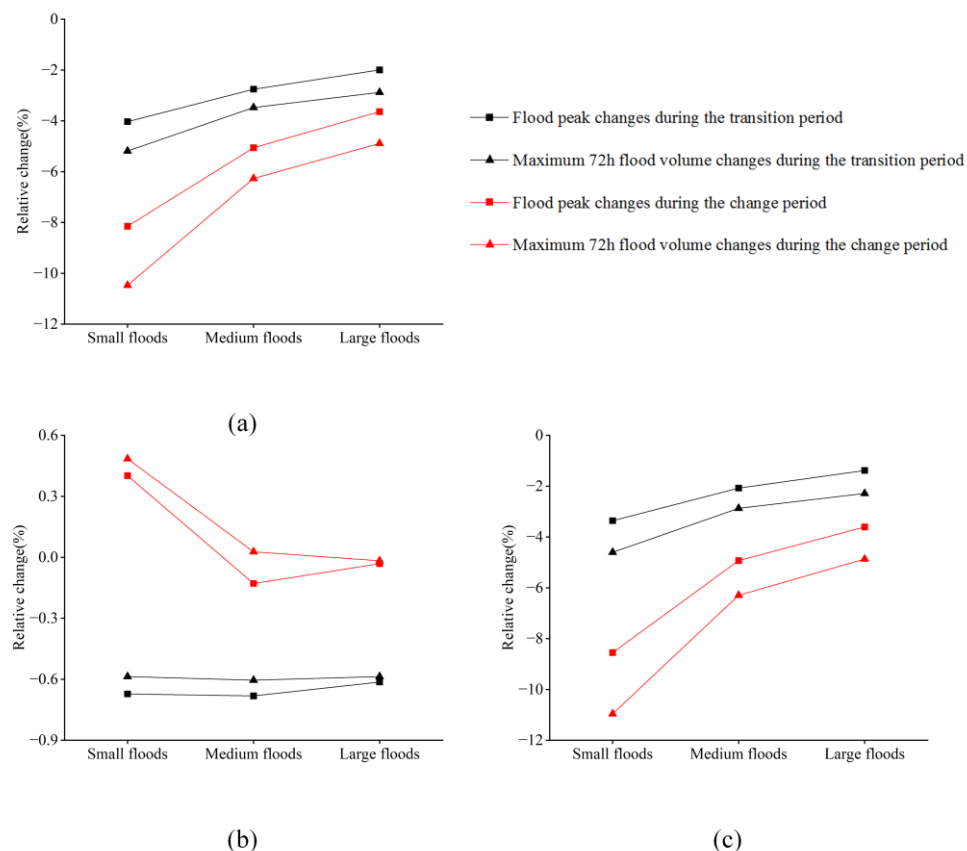


**Figure 7.** The impacts of the various USC scenarios on the floods of different magnitudes: (a) USC scenarios, (b) LUC scenarios, and (c) SWCM scenarios.

## 6. Conclusions

In this study, HEC-HMS models were constructed using DEM, soil, land use, rainfall, and hydrological data for the Taojiang River Basin for three periods, namely, 1981–1992 (baseline period), 1993–2007 (transition period), and 2008–2020 (change period), to analyze the impacts of the USC scenarios, LUC scenarios, and SWCM scenarios on floods in this basin. The primary conclusions of this study are as follows.

(1) By combining automatic and manual calibration models to optimize the parameters, the QR of the flood simulation results reached 70% for each period, with an average DC of greater than 0.7, resulting in a Grade B forecasting accuracy, indicating that the HEC-HMS model has an excellent applicability within the Taojiang River Basin.

(2) By adjusting the model parameters, the historical flood processes were simulated under different scenarios, and comparisons of the flood peak and maximum 72 h flood volume were conducted under the different scenarios. The results revealed that the USC scenarios led to decreases in both the flood peak and the maximum 72 h flood volume from 1981 to 2020. Specifically, compared with the baseline period, during the transition period, the flood peak maximum 72 h flood volume decreased by 3.06% and 4.00%. During the change period, these values decreased by 5.92% and 7.58%. The contribution of the LUC scenarios to these changes was relatively minor. This is primarily attributed to the SWCM scenarios, which played a dominant role in the USC scenarios in the Taojiang River Basin.

(3) We analyzed and quantified the relationship between the impacts of the USC scenarios, LUC scenarios, and SWCM scenarios on the floods and their magnitudes. The results show that compared with the baseline period, during the transition period, the USC scenarios led to decreases of 4.03%, 2.75%, and 2.00% in flood peaks of the small, medium, and large floods, respectively, and decreases of 5.19%, 3.48%, and 2.87% in the maximum 72 h flood volume, respectively. Similarly, during the change period, the flood peaks decreased by 8.15%, 5.06%, and 3.64%, and the maximum 72 h flood volume decreased by 10.47%, 6.27%, and 4.89%. Except for

the impacts of the LUCs on the floods during the transition period compared with the baseline period, which were not related to the magnitude of the floods, under the other scenarios, the impacts tended to decrease with increasing flood magnitude.

**Author Contributions:** Y.X., J.C. and J.Z. processed the data. Y.X., T.W., P.G. and F.X. designed the research. Y.X. and T.W. wrote the manuscript. T.W. and B.X. revised the manuscript. All authors have read and agreed to the published version of the manuscript.

**Funding:** This research was financially supported by the National Natural Science Foundation of China (NSFC Grant 52169001), the Great Science and Technology Project of the Ministry of Water Resources, PRC (SKS-2022010), the Water Resources Science and Technology Project of Jiangxi, China (202325ZDKT14), and the Open Research Fund supported by Jiangxi Province Institute of Water Sciences (2021SKSH01, 2023SKSH03).

**Data Availability Statement:** The rainfall data and hydrological data used in this research are non-public data.

**Conflicts of Interest:** The authors declare no conflicts of interest.

## Appendix A

**Table A1.** The impact of the USCs on partial floods.

Flood Number	Flood Peak ( $\text{m}^3/\text{s}$ )					Maximum 72 h Flood Volume (mm)				
	Baseline Period	Transition Period	Relative Change (%)	Change Period	Relative Change (%)	Baseline Period	Transition Period	Relative Change (%)	Change Period	Relative Change (%)
19810606	2250.4	2213.9	-1.62	2209.2	-1.83	54.03	52.45	-2.92	52.16	-3.46
19840428	1276	1215	-4.78	1142.5	-10.46	29.49	27.92	-5.32	26.19	-11.19
19850627	2304.9	2233.6	-3.09	2129.3	-7.62	43.34	41.36	-4.57	39.41	-9.07
19850925	1681.2	1632.1	-2.92	1554.6	-7.53	33.06	31.18	-5.69	29.23	-11.58
19860606	2026.5	1964.5	-3.06	1914.1	-5.55	54.01	52.32	-3.13	51.03	-5.52
19940621	4590	4495	-2.07	4472.9	-2.55	104.87	102.44	-2.32	101.5	-3.21
19950618	2753	2703.7	-1.79	2660.1	-3.37	65.02	62.74	-3.51	61	-6.18
19960803	2342.7	2269	-3.15	2191.4	-6.46	52.31	50.23	-3.98	47.91	-8.41
19980310	3039.3	3011.3	-0.92	2989.7	-1.63	80.32	77.73	-3.22	75.75	-5.69
20010511	1303.5	1227.6	-5.82	1213.5	-6.90	28.53	27.02	-5.29	25.48	-10.69
20080614	2333.5	2260.2	-3.14	2203.4	-5.58	52.34	50.24	-4.01	48.37	-7.59
20090704	2612.2	2530.3	-3.14	2443.4	-6.46	42.72	40.7	-4.73	39.19	-8.26
20100616	2292.6	2221.3	-3.11	2172.3	-5.25	61.14	59.64	-2.45	58.68	-4.02
20110517	2702.5	2652.8	-1.84	2638	-2.39	63.93	62.02	-2.99	60.68	-5.08
20120317	2028.8	1958.7	-3.46	1915.6	-5.58	47.94	46.2	-3.63	44.74	-6.68

**Table A2.** The impact of the LUCs on partial floods.

Flood Number	Flood Peak ( $\text{m}^3/\text{s}$ )					Maximum 72 h Flood Volume (mm)				
	Baseline Period	Transition Period	Relative Change (%)	Change Period	Relative Change (%)	Baseline Period	Transition Period	Relative Change (%)	Change Period	Relative Change (%)
19810606	2250.4	2238.1	-0.55	2248.7	-0.08	54.03	53.74	-0.54	53.96	-0.13
19840428	1276	1268.6	-0.58	1285.2	0.72	29.49	29.34	-0.51	29.72	0.78
19850627	2304.9	2292.4	-0.54	2317.9	0.56	43.34	43.14	-0.46	43.64	0.69
19850925	1681.2	1670.9	-0.61	1695	0.82	33.06	32.86	-0.60	33.3	0.73
19860606	2026.5	2010.6	-0.78	2021.2	-0.26	54.01	53.65	-0.67	54.04	0.06
19940621	4517.5	4495	-0.50	4512.9	-0.10	102.92	102.44	-0.47	102.85	-0.07
19950618	2720.7	2703.7	-0.62	2724.2	0.13	63.12	62.74	-0.60	63.16	0.06
19960803	2278.1	2269	-0.40	2291.5	0.59	50.42	50.23	-0.38	50.69	0.54
19980310	3028.3	3011.3	-0.56	3028.3	0.00	78.21	77.73	-0.61	78.14	-0.09
20010511	1284.9	1277.6	-0.57	1292.9	0.62	27.16	27.02	-0.52	27.33	0.63
20080614	2203.7	2187	-0.76	2203.7	0.00%	48.35	48.01	-0.70	48.37	0.04
20090704	2467.1	2444.9	-0.90	2443.4	-0.96%	39.43	39.12	-0.79	39.19	-0.61
20100616	2180.2	2163.1	-0.78	2172.3	-0.36%	58.71	58.35	-0.61	58.68	-0.05
20110517	2643	2625.2	-0.67	2638	-0.19%	60.71	60.32	-0.64	60.68	-0.05
20120317	1923.4	1908.8	-0.76	1915.6	-0.41%	44.81	44.52	-0.65	44.74	-0.16

**Table A3.** The impacts of the various USC scenarios on the floods of different magnitudes.

Flood Types	USCs				LUCs				SWCMs			
	Relative Change in Flood Peak (%)		Relative Change in Maximum 72 h Flood Volume (%)		Relative Change in Flood Peak (%)		Relative change in Maximum 72 h Flood Volume (%)		Relative Change in Flood Peak (%)		Relative Change in Maximum 72 h Flood Volume (%)	
	Transition Period	Change Period	Transition Period	Change Period	Transition Period	Change Period	Transition Period	Change Period	Transition Period	Change Period	Transition Period	Change Period
Small flood	−4.03	−8.15	−5.19	−10.47	−0.67	0.40	0.59	0.49	−3.36	−8.55	−4.60	−10.96
Medium flood	−2.75	−5.06	−3.48	−6.27	−0.68	−0.13	−0.60	0.03	−2.07	−4.93	−2.87	−6.29
Large flood	−2.00	−3.64	−2.87	−4.89	−0.61	−0.03	−0.59	−0.02	−1.38	−3.61	−2.29	−4.87

## References

- Yang, D.; Yang, Y.; Xia, J. Hydrological Cycle and Water Resources in a Changing World: A Review. *Geogr. Sustain.* **2021**, *2*, 115–122. [[CrossRef](#)]
- Prokešová, R.; Horáčková, Š.; Snopková, Z. Surface Runoff Response to Long-Term Land Use Changes: Spatial Rearrangement of Runoff-Generating Areas Reveals a Shift in Flash Flood Drivers. *Sci. Total Environ.* **2022**, *815*, 151591. [[CrossRef](#)] [[PubMed](#)]
- Feng, B.; Zhang, Y.; Bourke, R. Urbanization Impacts on Flood Risks Based on Urban Growth Data and Coupled Flood Models. *Nat. Hazards* **2021**, *106*, 613–627. [[CrossRef](#)]
- Le Floch, N.; Pons, V.; Hassan Abdalla, E.M.; Alfredsen, K. Catchment Scale Effects of Low Impact Development Implementation Scenarios at Different Urbanization Densities. *J. Hydrol.* **2022**, *612*, 128178. [[CrossRef](#)]
- Zhao, Y.; Xia, J.; Xu, Z.; Qiao, Y.; Shen, J.; Ye, C. Impact of Urbanization on Regional Rainfall-Runoff Processes: Case Study in Jinan City, China. *Remote Sens.* **2023**, *15*, 2383. [[CrossRef](#)]
- Guoyi, L.; Liu, J.; Shao, W. Urban Flood Risk Assessment under Rapid Urbanization in Zhengzhou City, China. *Reg. Sustain.* **2023**, *4*, 332–348. [[CrossRef](#)]
- Janizadeh, S.; Chandra Pal, S.; Saha, A.; Chowdhuri, I.; Ahmadi, K.; Mirzaei, S.; Mosavi, A.H.; Tiefenbacher, J.P. Mapping the Spatial and Temporal Variability of Flood Hazard Affected by Climate and Land-Use Changes in the Future. *J. Environ. Manag.* **2021**, *298*, 113551. [[CrossRef](#)] [[PubMed](#)]
- Xiao, L.; Robinson, M.; O’Connor, M. Woodland’s Role in Natural Flood Management: Evidence from Catchment Studies in Britain and Ireland. *Sci. Total Environ.* **2022**, *813*, 151877. [[CrossRef](#)]
- Luo, J.; Zhou, X.; Rubinato, M.; Li, G.; Tian, Y.; Zhou, J. Impact of Multiple Vegetation Covers on Surface Runoff and Sediment Yield in the Small Basin of Nverzhai, Hunan Province, China. *Forests* **2020**, *11*, 329. [[CrossRef](#)]
- Ghalehtemouri, K.J.; Ros, F.C.; Rambat, S. Flood Risk Assessment through Rapid Urbanization LULC Change with Destruction of Urban Green Infrastructures Based on NASA Landsat Time Series Data: A Case of Study Kuala Lumpur between 1990–2021. *Acta Ecol Sin.* **2023**, in press. [[CrossRef](#)]
- Gabriels, K.; Willems, P.; Van Orshoven, J. A Comparative Flood Damage and Risk Impact Assessment of Land Use Changes. *Nat. Hazards Earth Syst. Sci.* **2022**, *22*, 395–410. [[CrossRef](#)]
- Liu, Y.; Han, J.; Jiao, J.; Liu, B.; Ge, W.; Pan, Q.; Wang, F. Responses of Flood Peaks to Land Use and Landscape Patterns under Extreme Rainstorms in Small Catchments—A Case Study of the Rainstorm of Typhoon Lekima in Shandong, China. *Int. Soil Water Conserv. Res.* **2022**, *10*, 228–239. [[CrossRef](#)]
- Du, X.; Jian, J.; Du, C.; Stewart, R.D. Conservation Management Decreases Surface Runoff and Soil Erosion. *Int. Soil Water Conserv. Res.* **2022**, *10*, 188–196. [[CrossRef](#)]
- Yaekob, T.; Tamene, L.; Gebrehiwot, S.G.; Demissie, S.S.; Adimassu, Z.; Woldearegay, K.; Mekonnen, K.; Amede, T.; Abera, W.; Recha, J.W.; et al. Assessing the Impacts of Different Land Uses and Soil and Water Conservation Interventions on Runoff and Sediment Yield at Different Scales in the Central Highlands of Ethiopia. *Renew. Agric. Food Syst.* **2022**, *37*, S73–S87. [[CrossRef](#)]
- Liu, Y.; Han, J.; Liu, Y.; Zhang, S.; Min, L.; Liu, B.; Jiao, J.; Zhang, L. Effects of Soil and Water Conservation Measures of Slope Surfaces on Flood Peaks of Small Watersheds: A Study Based on Three Extreme Rainstorm Events in Northern China. *CATENA* **2023**, *232*, 107432. [[CrossRef](#)]
- Zhao, Y.; Cao, W.; Hu, C.; Wang, Y.; Wang, Z.; Zhang, X.; Zhu, B.; Cheng, C.; Yin, X.; Liu, B.; et al. Analysis of Changes in Characteristics of Flood and Sediment Yield in Typical Basins of the Yellow River under Extreme Rainfall Events. *CATENA* **2019**, *177*, 31–40. [[CrossRef](#)]
- Fu, S.; Yang, Y.; Liu, B.; Liu, H.; Liu, J.; Liu, L.; Li, P. Peak Flow Rate Response to Vegetation and Terraces under Extreme Rainstorms. *Agric. Ecosyst. Environ.* **2020**, *288*, 106714. [[CrossRef](#)]
- Zhu, T.X. Effectiveness of Conservation Measures in Reducing Runoff and Soil Loss Under Different Magnitude–Frequency Storms at Plot and Catchment Scales in the Semi-Arid Agricultural Landscape. *Environ. Manag.* **2016**, *57*, 671–682. [[CrossRef](#)]

19. Yuan, F.; Yang, G.; Zhang, Q.; Li, H. Soil Erosion Assessment of the Poyang Lake Basin, China: Using USLE, GIS and Remote Sensing. *J. Remote Sens. GIS* **2016**, *5*, 12. [[CrossRef](#)]
20. Li, X.; Hu, Q.; Zhang, Q.; Wang, R. Response of Rainfall Erosivity to Changes in Extreme Precipitation in the Poyang Lake Basin, China. *J. Soil Water Conserv.* **2020**, *75*, 537–548. [[CrossRef](#)]
21. Wen, T.; Xiong, L.; Jiang, C.; Xu, X.; Liu, Z. Attribution analysis of annual sediment load of Ganjiang River Basin using BMA based on time-varying moment models. *Trans. Chin. Soc. Agric. Eng.* **2021**, *37*, 140–149. (In Chinese)
22. Keller, A.A.; Garner, K.; Rao, N.; Knipping, E.; Thomas, J. Hydrological Models for Climate-Based Assessments at the Watershed Scale: A Critical Review of Existing Hydrologic and Water Quality Models. *Sci. Total Environ.* **2023**, *867*, 161209. [[CrossRef](#)] [[PubMed](#)]
23. Hamdan, A.N.A.; Almuktar, S.; Scholz, M. Rainfall-Runoff Modeling Using the HEC-HMS Model for the Al-Adhaim River Catchment, Northern Iraq. *Hydrology* **2021**, *8*, 58. [[CrossRef](#)]
24. Guduru, J.U.; Jilo, N.B.; Rabba, Z.A.; Namara, W.G. Rainfall-Runoff Modeling Using HEC-HMS Model for Meki River Watershed, Rift Valley Basin, Ethiopia. *J. Afr. Earth Sci.* **2023**, *197*, 104743. [[CrossRef](#)]
25. Azam, M.; Kim, H.S.; Maeng, S.J. Development of Flood Alert Application in Mushim Stream Watershed Korea. *Int. J. Disaster Risk Reduct.* **2017**, *21*, 11–26. [[CrossRef](#)]
26. Lin, Q.; Lin, B.; Zhang, D.; Wu, J. Web-Based Prototype System for Flood Simulation and Forecasting Based on the HEC-HMS Model. *Environ. Model. Softw.* **2022**, *158*, 105541. [[CrossRef](#)]
27. Tu, H.; Wang, X.; Zhang, W.; Peng, H.; Ke, Q.; Chen, X. Flash Flood Early Warning Coupled with Hydrological Simulation and the Rising Rate of the Flood Stage in a Mountainous Small Watershed in Sichuan Province, China. *Water* **2020**, *12*, 255. [[CrossRef](#)]
28. Patel, P.; Thakur, P.K.; Aggarwal, S.P.; Garg, V.; Dhote, P.R.; Nikam, B.R.; Swain, S.; Al-Ansari, N. Revisiting 2013 Uttarakhand Flash Floods through Hydrological Evaluation of Precipitation Data Sources and Morphometric Prioritization. *Geomat. Nat. Hazards Risk* **2022**, *13*, 646–666. [[CrossRef](#)]
29. Davtalab, R.; Mirchi, A.; Khatami, S.; Gyawali, R.; Massah, A.; Farajzadeh, M.; Madani, K. Improving Continuous Hydrologic Modeling of Data-Poor River Basins Using Hydrologic Engineering Center’s Hydrologic Modeling System: Case Study of Karkheh River Basin. *J. Hydrol. Eng.* **2017**, *22*, 05017011. [[CrossRef](#)]
30. Ben Khéifa, W.; Mosbahi, M. Modeling of Rainfall-Runoff Process Using HEC-HMS Model for an Urban Ungauged Watershed in Tunisia. *Model. Earth Syst. Environ.* **2022**, *8*, 1749–1758. [[CrossRef](#)]
31. Younis, S.M.Z.; Ammar, A. Quantification of Impact of Changes in Land Use-Land Cover on Hydrology in the Upper Indus Basin, Pakistan. *Egypt. J. Remote Sens. Space Sci.* **2018**, *21*, 255–263. [[CrossRef](#)]
32. Yan, X.; Lin, M.; Chen, X.; Yao, H.; Liu, C.; Lin, B. A New Method to Restore the Impact of Land-use Change on Flood Frequency Based on the Hydrologic Engineering Center-Hydrologic Modelling System Model. *Land Degrad. Dev.* **2020**, *31*, 1520–1532. [[CrossRef](#)]
33. Gao, Y.; Chen, J.; Luo, H.; Wang, H. Prediction of Hydrological Responses to Land Use Change. *Sci. Total Environ.* **2020**, *708*, 134998. [[CrossRef](#)] [[PubMed](#)]
34. Kabeja, C.; Li, R.; Guo, J.; Rwtangabo, D.E.R.; Manyifika, M.; Gao, Z.; Wang, Y.; Zhang, Y. Erratum: Kabeja, C.; et al. The Impact of Reforestation Induced Land Cover Change (1990–2017) on Flood Peak Discharge Using HEC-HMS Hydrological Model and Satellite Observations: A Study in Two Mountain Basins, China. *Water* **2021**, *13*, 676, Erratum in *Water* **2020**, *12*, 1347. [[CrossRef](#)]
35. Zhao, S.; Luo, P.; Liu, H. Spatial-temporal variation characteristics of different grades of rainfall in Taojiang River Basin along upper reaches of Ganjiang River. *J. Nanchang Inst. Technol.* **2022**, *41*, 32–39. (In Chinese)
36. Şengül, S.; İspirli, M.N. Predicting Snowmelt Runoff at the Source of the Mountainous Euphrates River Basin in Turkey for Water Supply and Flood Control Issues Using HEC-HMS Modeling. *Water* **2022**, *14*, 284. [[CrossRef](#)]
37. Rammal, M.; Berthier, E. Runoff Losses on Urban Surfaces during Frequent Rainfall Events: A Review of Observations and Modeling Attempts. *Water* **2020**, *12*, 2777. [[CrossRef](#)]
38. Gao, B.; Xu, Y.; Sun, Y.; Wang, Q.; Wang, Y.; Li, Z. The Impacts of Impervious Surface Expansion and the Operation of Polders on Flooding under Rapid Urbanization Processes. *Theor. Appl. Climatol.* **2023**, *151*, 1215–1225. [[CrossRef](#)]
39. Halwatura, D.; Najim, M.M.M. Application of the HEC-HMS Model for Runoff Simulation in a Tropical Catchment. *Environ. Model. Softw.* **2013**, *46*, 155–162. [[CrossRef](#)]
40. Tassew, B.G.; Belete, M.A.; Miegel, K. Application of HEC-HMS Model for Flow Simulation in the Lake Tana Basin: The Case of Gilgel Abay Catchment, Upper Blue Nile Basin, Ethiopia. *Hydrology* **2019**, *6*, 21. [[CrossRef](#)]
41. GB/T22482-2008; Standard for Hydrological Information and Hydrological Forecasting. CHINESE GB Standards: Beijing, China, 2008. (In Chinese)
42. Yao, C.; Chang, L.; Ding, J.; Li, Z.; An, D.; Zhang, Y. Evaluation of the Effects of Underlying Surface Change on Catchment Hydrological Response Using the HEC-HMS Model. *Proc. Int. Assoc. Hydrol. Sci.* **2014**, *364*, 145–150. [[CrossRef](#)]
43. Lehbab-Boukezzi, Z.; Boukezzi, L.; Errih, M. Uncertainty Analysis of HEC-HMS Model Using the GLUE Method for Flash Flood Forecasting of Mekerra Watershed, Algeria. *Arab. J. Geosci.* **2016**, *9*, 751. [[CrossRef](#)]
44. Natarajan, S.; Radhakrishnan, N. Simulation of Rainfall–Runoff Process for an Ungauged Catchment Using an Event-Based Hydrologic Model: A Case Study of Koraiyar Basin in Tiruchirappalli City, India. *J. Earth. Syst. Sci.* **2021**, *130*, 30. [[CrossRef](#)]

45. Glas, R.; Hecht, J.; Simonson, A.; Gazoorian, C.; Schubert, C. Adjusting Design Floods for Urbanization across Groundwater-Dominated Watersheds of Long Island, NY. *J. Hydrol.* **2023**, *618*, 129194. [[CrossRef](#)]
46. Wei, L.; Hu, K.; Hu, X. Rainfall Occurrence and Its Relation to Flood Damage in China from 2000 to 2015. *J. Mt. Sci.* **2018**, *15*, 2492–2504. [[CrossRef](#)]

**Disclaimer/Publisher's Note:** The statements, opinions and data contained in all publications are solely those of the individual author(s) and contributor(s) and not of MDPI and/or the editor(s). MDPI and/or the editor(s) disclaim responsibility for any injury to people or property resulting from any ideas, methods, instructions or products referred to in the content.